IOPscience iopscience.iop.org

Home Search Collections Journals About Contact us My IOPscience

A regularization of the Burgers equation using a filtered convective velocity

This article has been downloaded from IOPscience. Please scroll down to see the full text article.

2008 J. Phys. A: Math. Theor. 41 344016

(http://iopscience.iop.org/1751-8121/41/34/344016)

View the table of contents for this issue, or go to the journal homepage for more

Download details:
IP Address: 171.66.16.150
The article was downloaded on 03/06/2010 at 07:08

Please note that terms and conditions apply.

IOP PUBLISHING JOURNAL OF PHYSICS A: MATHEMATICAL AND THEORETICAL

J. Phys. A: Math. Theor. **41** (2008) 344016 (21pp) doi:10.1088/1751-8113/41/34/344016

A regularization of the Burgers equation using a filtered convective velocity

Greg Norgard and Kamran Mohseni

University of Colorado, Boulder, CO 80309, USA

E-mail: mohseni@colorado.edu

Received 7 December 2007, in final form 2 July 2008
Published 11 August 2008
Online at stacks.iop.org/JPhysA/41/344016

Abstract

This paper examines the properties of a regularization of the Burgers equation in one and multiple dimensions using a filtered convective velocity, which we have dubbed as the convectively filtered Burgers (CFB) equation. A physical motivation behind the filtering technique is presented. An existence and uniqueness theorem for multiple dimensions and a general class of filters is proven. Multiple invariants of motion are found for the CFB equation which are shown to be shared with the viscous and inviscid Burgers equations. Traveling wave solutions are found for a general class of filters and are shown to converge to weak solutions of the inviscid Burgers equation with the correct wave speed. Numerical simulations are conducted in 1D and 2D cases where the shock behavior, shock thickness and kinetic energy decay are examined. Energy spectra are also examined and are shown to be related to the smoothness of the solutions. This approach is presented with the hope of being extended to shock regularization of compressible Euler equations.

PACS numbers: 47.10.ab, 47.27.ep, 47.27.em, 47.40.−x

1. Introduction

The Euler and Navier–Stokes equations are well known as the fundamental laws governing fluid dynamics; yet even after 200 years they continue to present theoretical and computational challenges. The nonlinear terms inherent in the equations give rise to small-scale structures, in the form of turbulence and shocks, as shown in section 2, which have proven to be the bane of computational simulations. With the proper modeling of these small scales, we hope it is possible to address both turbulence and shocks with one encompassing technique. Currently, the Lagrangian averaging approach is making strides in handling turbulent flows [1–10]. That work motivated the work presented in this paper. The Lagrangian averaging approach results in a filtered convective velocity in the nonlinear term. This paper also uses a filtered convective

 © 2008 IOP Publishing Ltd Printed in the UK

velocity in the nonlinear term of the Burgers equation, with the intention of discovering if this technique is a reasonable means of capturing shock formation.

The Burgers equation has been a useful testing grounds for fluid dynamics for many years due to the fact that it shares the same nonlinear convective term as the Euler and Navier–Stokes equations. Indeed, the Burgers equation has been the focus of much work, both numerically and analytically [11–19]. Much like the Euler equations, the inviscid Burgers equation,

$$u_t + uu_x = 0, \tag{1}$$

can be expressed as a conservation law. Johannes Martinus Burgers regularized the inviscid Burgers equation with a dissipative viscous term creating the viscous Burgers equation,

$$u_t + uu_x = \nu u_{xx}. \tag{2}$$

This was originally intended as a simplistic model for one-dimensional turbulence [11, 12]. Both viscous and inviscid Burgers equations are easily extended into multiple dimensions giving

$$\mathbf{u}_t + \mathbf{u} \cdot \nabla \mathbf{u} = \nu \triangle \mathbf{u} \tag{3}$$

and

$$\mathbf{u}_t + \mathbf{u} \cdot \nabla \mathbf{u} = 0. \tag{4}$$

It is well established that the inviscid Burgers equation forms discontinuities in finite time, determined by initial conditions [14, 15]. To deal with these discontinuities weak solutions are introduced. However, when weak solutions are introduced, solutions are no longer necessarily unique [15, 20]. In order to choose the physically relevant solution, an entropy condition is applied, which one and only one weak solution satisfies. This physically relevant solution is referred to as the entropy solution. Lax, Oleinik and Kruzkov have examined the entropy condition for conservation laws and expressed it using different techniques [15, 20, 21]. Each of their entropy conditions can be used in different classes of conservation laws, but can all be applied to the inviscid Burgers equation with equivalent results [22].

With the dissipative term, the viscous Burgers equation does not form discontinuities [14, 15]. Indeed it smooths discontinuities found in initial conditions, and has a unique infinitely differentiable solution for all time [13, 23]. Moreover, the limit of the solutions as $\nu \to 0$ converge strongly to the entropy solution of the inviscid Burgers equation [15, 20, 21].

Addition of a viscous term in the form of a Laplacian is not the only technique for regularizing the inviscid Burgers equation, so that the limit of the solutions converge to the entropy solution. Many other regularizations have been proposed, typically with the addition of a dissipative term. Among them are regularizations with hyperviscosity, filtered viscosity and a combination of viscosity and dispersion [18, 24–27].

Another well-known regularized equation is the KDV equation which uses a dispersive term,

$$u_t + uu_x = -\epsilon u_{xxx}. \tag{5}$$

This regularizes the inviscid Burgers equation in the sense that solutions are now continuous, however, many oscillations form as $\epsilon \to 0$, requiring a weak limit for convergence [28, 29]. This limit is not the entropy solution, nor even a weak solution of the inviscid Burgers equation [30].

Connection to the LANS-α equation. The incompressible isotropic LANS-α equations are given by [9]

$$\frac{\partial \mathbf{u}}{\partial t} + \bar{\mathbf{u}} \cdot \nabla \mathbf{u} + u_j \nabla \bar{u}_j = -\nabla P + \frac{1}{Re} \triangle \mathbf{u}, \tag{6}$$

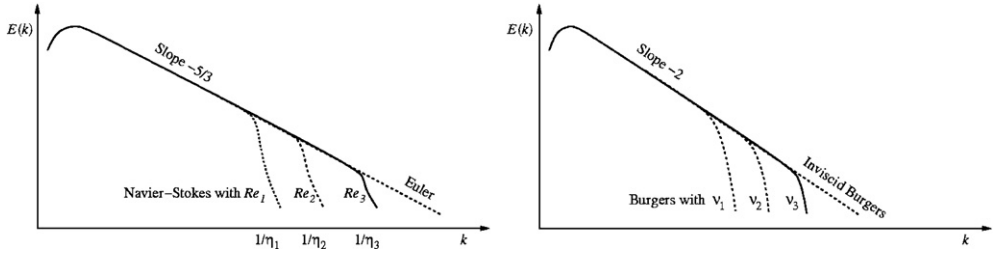

Figure 1. Schematics of energy cascade for the Navier–Stokes/Euler equations and the viscous/inviscid Burgers equation are shown. In an inviscid flow, both turbulence (*a*) and shocks (*b*) show continuous generation of higher wave modes indefinitely. (*a*) Energy cascades from high wavelengths to lower wavelengths at a predicted rate of $-\frac{5}{3}$ for the Navier–Stokes/Euler equations. For the Navier–Stokes equations, the kinetic energy drops drastically upon reaching a certain wavelength; the Kolmogorov scale, η. For the Euler equations the cascade continues on indefinitely. Here $Re_1 < Re_2 < Re_3$. (*b*) For the Burgers equation, shocks can form from continuous initial conditions. The energy cascade has a slope of -2 when shocks form, until viscosity begins to exert its influence and balance the steepening effect of the nonlinear term. Here $\nu_3 < \nu_2 < \nu_1$.

where $\mathbf{u}$ is defined as

$$\mathbf{u} = \bar{\mathbf{u}} - \alpha^2 \triangle \bar{\mathbf{u}}.$$

As mentioned earlier, this equation has had success capturing some of the behavior for a class of turbulent flows. It can be seen in equation (6) that LANS-α employs a filtered convective velocity. What this paper proposes is that it is this filtered convective velocity in the nonlinear term that is successful in modeling small-scale behavior. As explained in section 2 and figure 1, both turbulence and shocks are a result of such small-scale behavior. If such a term can in fact successfully handle all small-scale effects, then such a term could also be used to model shocks alongside turbulence.

This paper begins the examination of using such a nonlinear term in shock regularization. As was stated, the Burgers equation has been extensively researched and is well understood. It has been chosen as a testing ground for using a filtered convective velocity for shock regularization due to its well-understood shock formations. This technique is not intended to be an analytically or numerically superior method of regularizing shocks, but more as a proof of concept. If the averaging of the convective velocity can be shown to be effective in regularizing shocks, then perhaps it would be possible to develop a technique based on this that would capture both shock and turbulent behavior in more complicated flows.

This paper considers what will be referred to as the convectively filtered Burgers equation (CFB), where the convective velocity in the inviscid Burgers equation is replaced with a filtered (averaged) velocity. The filtering is done by convoluting the velocity u with the kernel g (properties of which will be discussed in section 3) resulting in

$$u_t + \bar{u}u_x = 0 \tag{7a}$$

$$\bar{u} = g * u. \tag{7b}$$

If an inverse for the filtering exists, the equation, using only the filtered velocity, can be rewritten as

$$\bar{u}_t + \bar{u}\bar{u}_x = \overline{g^{-1}(\bar{u}\bar{u}_x) - \bar{u}g^{-1}(\bar{u}_x)}, \tag{8}$$

where g^{-1} represents the inverse of the low-pass filter. Equation (8) reformulates equations (7*a*) and (7*b*) into an equation analogous to the large eddy simulation (LES) [31–33]. To this end the right-hand side of equation (8) can be considered a convective subgrid scale stress for regularizing a shock.

This being said, it is the intention that the filtered velocity, $\bar{u}$, be considered the physically relevant quantity, that captures the proper macroscopic, or low wavemode, behavior. Comparing equation (8) with equation (2), the right-hand side of equation (8) replaces viscosity as the regularizing term. As such, it is $\bar{u}$ from the CFB equations that will be compared to the velocity from the viscous Burgers equation. The unfiltered velocity, u, is used primarily as an analytical tool. As it is unfiltered, it contains both low and high wavemode activity. In section 5, most of the invariants of motion found for CFB involve the unfiltered velocity.

CFB, like Burgers equation, is easily extended into multiple dimensions, with equations

$$\mathbf{u}_t + \bar{\mathbf{u}} \cdot \nabla \mathbf{u} = 0 \tag{9a}$$

$$\bar{\mathbf{u}} = g * \mathbf{u}. \tag{9b}$$

Special attention is paid to the Helmholtz filter, which gains notice for several reasons. It is a common filter, employed in the Leray-α model of turbulence [1–3], Lagrangian-averaged Navier–Stokes (LANS-α) [4–6, 34] and in the Lagrangian-averaged Euler-α [8, 9]. It has been shown that one-dimensional CFB is Hamiltonian when the Helmholtz filter is used [35, 36]. Also, the inverse of the Helmholtz filter is known for vanishing or periodic boundary conditions, so it can be expressed through convolution or using differential notation. In 1D, the following are equivalent:

$$\bar{u} = \tfrac{1}{2} e^{-|\cdot|} * u \tag{10a}$$

$$u = \bar{u} - \bar{u}_{xx}. \tag{10b}$$

When moving to higher dimensions the convolution kernel changes and the double derivative becomes a Laplacian. Using the Helmholtz filter, equation (8) can be simplified to

$$\bar{u}_t + \bar{u}\bar{u}_x = -3\alpha^2 \left(I - \alpha^2 \partial_x^2\right)^{-1} (\bar{u}_x \bar{u}_{xx}). \tag{11}$$

The CFB equation is not the first look into the use of filtered convective velocities. Jean Leray proposed using a filtered convective velocity in the Navier–Stokes equations as early as 1934 [37]. This was done in an attempt at proving that regular solutions to the Navier–Stokes equations exist and to examine properties of those solutions. This has led to several investigations into the Leray-α model of turbulence [1, 38, 39] primarily using the Helmholtz filter. In the projected models for extending our technique into the Euler equations, the filtering occurs in more than just the convective velocity. At that point the research loses much of the similarity with Leray's work. This extension into Euler equations will be the topic of following papers.

Special cases of the CFB equation have been previously studied. The family of equations

$$u_t + \bar{u}u_x + bu\bar{u}_x = 0,$$
$$\bar{u} = g * u,$$

where b was a free parameter, has been examined [35, 40], where g was almost exclusively the Helmholtz filter. The $b = 0$ case reduces to the 1D version of CFB. Holm and Staley [35] established the invariant quantities, $\int u$ and $\|u\|_\infty$. They examined peakon solutions and cliff solutions both analytically and numerically. A Lagrangian structure was shown for the $b \neq 0$ case and a Hamiltonian structure proposed for $b = 0$ by Degasperis *et al* [40]. Bhat

and Fetecau [36] also examined one-dimensional CFB with the Helmholtz filter. They more fully established the Hamiltonian structure proposed by Degasperis *et al*. They also proved the existence and uniqueness of a solution, and proved that the solutions converge to a weak solution of the inviscid Burgers equation.

This paper extends the results into the use of more general filters and looks into 1D and multiple dimensions. It also examines many of the physically relevant characteristics of CFB. Some of the results in this paper have been previously presented in conference papers [7, 41, 42]. The following section elaborates on the motivation for the averaging (filtering) technique. Section 3 establishes the characteristics desired in the filter. Existence and uniqueness theorems are given in section 4 for CFB in multiple dimensions and a general class of filters. Section 5 examines the various invariants of motion for CFB and compares them to those found in viscous and inviscid Burgers equations. In section 6, a traveling wave solution for general filters is presented and analyzed. Sections 7–10 deal with numerical simulations and results regarding shock behavior, spectral energy and energy norms. All is then followed with concluding remarks.

2. Similarities in high wave numbers for inviscid turbulence and shocks

We begin by examining the mechanics behind shock formation and turbulence. The nonlinear convective term $\mathbf{u}\cdot\nabla\mathbf{u}$ generates high wave modes, by transferring energy into smaller scales as time progresses. This term can be found in the Euler and Navier–Stokes equations, where it is responsible for tilting and stretching of vortical structures [43]. It is also found in the Burgers equation. If this cascade of energy into the smaller scales is left unchecked, discontinuities will form. To prevent this, viscosity is added. Dependent on the Reynolds number, there exists a length scale, the Kolmogorov scale, where viscosity begins to dominate the energy cascade, transferring kinetic energy into thermal energy through dissipation. In the Navier–Stokes equation, the energy cascade has a slope of $-\frac{5}{3}$ until the Kolmogorov scale, illustrated in figure 1(*a*). The viscous Burgers equation has an energy cascade slope of -2 until viscosity begins to dominate; seen in figure 1(*b*) [44, 45]. The Euler equations and the inviscid Burgers equation are the respective limits as viscosity goes to zero. By filtering the convective velocity, the energy cascade is affected through the nonlinear term. A low-pass filtered velocity will have less energy in the high wave modes, thus the nonlinear term $\bar{\mathbf{u}}\cdot\nabla\mathbf{u}$ will generate higher wave modes at a reduced rate. By reducing the energy cascade, discontinuities are prevented from forming.

This physical argument has been our motivation for the last few years for an inviscid regularization technique that could simultaneously regularize the high wave mode problem in both turbulence and shocks.

3. Filters

In equation (9*b*), the filtered velocity is obtained by convoluting the unfiltered velocity $\mathbf{u}$ with a low-pass filter g. This section discusses the requirements and properties of the low-pass filter. Using physical and analytical arguments the class of relevant filters is outlined.

3.1. Filtering as a weighted average

From a physical perspective, equations (9*a*) and (9*b*) describe a fluid where the convective velocity of a particle is the weighted average of the velocities of the particles around it. In such an averaging, there are several guidelines that seem intuitively reasonable. The averaging

Table 1. This table succinctly lists the requirements of the low-pass filters employed in equation (9*b*).

Properties	Mathematical expression
Normalized	$\int g = 1$
Non-negative	$g(\mathbf{x}) > 0, \forall \mathbf{x}$
Decreasing	$\lvert\mathbf{x}_1\rvert \geqslant \lvert\mathbf{x}_2\rvert \Rightarrow g(\mathbf{x}_1) \geqslant g(\mathbf{x}_2)$
Symmetric	$\lvert\mathbf{x}_1\rvert = \lvert\mathbf{x}_2\rvert \Rightarrow g(\mathbf{x}_1) = g(\mathbf{x}_2)$
Fourier decay	$\lim_{\lvert\mathbf{k}\rvert\to\infty} \lvert\mathbf{k}\rvert\hat{g}(\mathbf{k}) = 0$

should give no particle a negative weight, should give no directional preference, and should give more weight to particles that are physically closer. These guidelines are easily expressed as mathematical properties of the filter. Thus g should be non-negative, decreasing and radially symmetric. Furthermore, as a weighted average the integral of g over the domain should be precisely one. These conditions are succintly listed in table 1.

3.2. Characteristic wavelength parameter

Each such filter g is equipped with a parameter α, such that α is the characteristic wavelength of that filter. This parameter is introduced by scaling the filter as such,

$$g^\alpha = \frac{1}{\alpha} g\left(\frac{\mathbf{x}}{\alpha}\right).$$

This scaling is also realized in the Fourier domain by noting that

$$\widehat{g^\alpha}(\mathbf{k}) = \widehat{g}(\alpha\mathbf{k}). \tag{12}$$

Thus as α becomes smaller, the wavelength where the filter exerts influence also become smaller.

With this scaling, the filter remains normalized, non-negative, decreasing and isotropic. Furthermore as $\alpha \to 0$, g^α approaches the Dirac delta function, and equation (9*a*) formally limits to the inviscid Burgers equation. This parameter is crucial in resolving features in $\bar{\mathbf{u}}$. When convoluting g^α with $\mathbf{u}$, features in $\mathbf{u}$ that have length less than α will be smoothed out. It is also seen in section 8.3 that α controls shock thickness.

3.3. Fourier decay properties

In the following section, theorem 4.1 states that system (16*a*)–(16*c*) has a continuously differentiable solution, if $g(\mathbf{x}) \in W^{1,1}(\mathbb{R}^n)$ or alternatively

$$\|g\|_{L^1} < \infty, \tag{13}$$

and

$$\left\| \frac{\partial}{\partial x_j} g \right\|_{L^1} < \infty. \tag{14}$$

Condition (14) has implication in the Fourier domain. The Riemann–Lebesgue lemma demands that if $\frac{\partial}{\partial x_j} g \in L^1$ then $\widehat{\frac{\partial}{\partial x_j} g} = ik_j\hat{g} \in C_0$. Thus not only must $\hat{g} \in C_0$, but the condition,

$$\lim_{|\mathbf{k}|\to\infty} |\mathbf{k}|\hat{g}(\mathbf{k}) = 0, \tag{15}$$

must be satisfied in order to meet (14). Note that (15) is a necessary, not sufficient, condition to meet theorem 4.1.

4. Existence and uniqueness theorem

It has been previously proven [36] that the initial-value problem (16*a*)–(16*c*) using the Helmholtz filter (10*a*) has a continuously differentiable solution for continuously differentiable initial conditions. Taking inspiration from that work, the following theorem generalizes the existence and uniqueness result into multiple dimensions and a variety of filters.

Theorem 4.1. *Let* $g(\mathbf{x}) \in W^{1,1}(\mathbb{R}^n)$ *and* $\mathbf{u}_0(\mathbf{x}) \in C^1(\mathbb{R}^n)$*, then there exists a unique global solution* $\mathbf{u}(\mathbf{x}, t) \in C^1(\mathbb{R}^n, \mathbb{R})$ *to the initial-value problem (16a)–(16c).*

$$\mathbf{u}_t + \bar{\mathbf{u}} \cdot \nabla \mathbf{u} = 0 \tag{16a}$$

$$\bar{\mathbf{u}} = g * \mathbf{u} \tag{16b}$$

$$\mathbf{u}(\mathbf{x}, 0) = \mathbf{u}_0(\mathbf{x}). \tag{16c}$$

Proof. Begin by shifting perspective into the material view. Associate a map $\phi(\boldsymbol{\xi}, t) : \mathbb{R}^n \to \mathbb{R}^n$ as the map from a particle's original position, $(\boldsymbol{\xi})$, to the particle's position at time t, $(\mathbf{x})$. Naturally this dictates that $\phi(\boldsymbol{\xi}, 0) = \boldsymbol{\xi}$. Associate this material map with the velocity $\bar{\mathbf{u}}$ by

$$\frac{\partial}{\partial t}\phi(\boldsymbol{\xi}, t) = \bar{\mathbf{u}}(\phi(\boldsymbol{\xi}, t), t). \tag{17}$$

It can then be seen that (16*a*) simply becomes

$$\frac{\partial}{\partial t}\mathbf{u}(\phi(\boldsymbol{\xi}, t), t) = 0, \tag{18}$$

and thus, $\mathbf{u}(\phi(\boldsymbol{\xi}, t), t) = \mathbf{u}(\phi(\boldsymbol{\xi}, 0), 0) = \mathbf{u}_0(\boldsymbol{\xi})$, which implies

$$\|\mathbf{u}\|_{L^\infty} = \|\mathbf{u}_0\|_{L^\infty}. \tag{19}$$

If it is assumed that $\phi(\boldsymbol{\xi}, t)$ has a continuously differentiable inverse $\phi^{-1}(\mathbf{x}, t)$, then (16*a*)–(16*c*) will have the continuously differentiable solution

$$\mathbf{u}(\mathbf{x}, t) = \mathbf{u}_0(\phi^{-1}(\mathbf{x}, t)). \tag{20}$$

A sufficient condition for such a ϕ^{-1} to uniquely exist is the Jacobian of ϕ to be nonzero for all positions and time. Thus if $J(\phi(\boldsymbol{\xi})) \neq 0$, $\forall \boldsymbol{\xi}, t$, then (16*a*)–(16*c*) is uniquely solved by (20).

Using a result from Aris [46], the time derivative of the Jacobian is found to be

$$\frac{\partial}{\partial t}J = \nabla \cdot \bar{\mathbf{u}} J, \tag{21}$$

which is a differentiable equation with solution

$$J = J_0 \exp\left(\int_0^t \nabla \cdot \bar{\mathbf{u}}\, \mathrm{d}t\right). \tag{22}$$

Clearly $J_0 = 1$, since $\phi(\boldsymbol{\xi}, 0) = \boldsymbol{\xi}$. Thus it is clear that J remains nonzero if $\left|\int_0^t \nabla \cdot \bar{\mathbf{u}}\, \mathrm{d}t\right| < \infty$.

Given that $g(\mathbf{x}) \in W^{1,1}(\mathbb{R}^n)$, there exists $M \in \mathbb{R}$, such that

$$\left\| \frac{\partial}{\partial x_i} g \right\|_{L^1} \leqslant M < \infty, \qquad \forall i. \tag{23}$$

Knowing that $\frac{\partial}{\partial x_i} g \in L^1$ and $\mathbf{u} \in L^\infty$, we know that $\frac{\partial}{\partial x_i}\bar{u}_j$ exists and that

$$\frac{\partial}{\partial x_i}\bar{u}_j = \frac{\partial}{\partial x_i} g * u_j.$$

Table 2. This table lists the additional constraints, the modified equations and the corresponding invariants of motion for the viscous, inviscid and convectively filtered Burgers equations.

Additional constraints	System equations	Invariants of motion
	Viscous Burgers	
One dimensional	$u_t + uu_x = \nu u_{xx}$	$\int u$
Potential function	$\mathbf{u}_t + \mathbf{u}\cdot\nabla\mathbf{u} = \nu \triangle \mathbf{u}$, $\mathbf{u} = \nabla\phi$	$\int u_i$
	Inviscid Burgers	
One dimensional	$u_t + uu_x = 0$	$\int u^n, \forall n \in \mathbb{Z}$
Potential Function	$\mathbf{u}_t + \mathbf{u}\cdot\nabla\mathbf{u} = 0$, $\mathbf{u} = \nabla\phi$	$\int u_i$
Continuity Equation	$\mathbf{u}_t + \mathbf{u}\cdot\nabla\mathbf{u} = 0$, $\rho_t + \nabla(\rho\mathbf{u}) = 0$	$\int \rho, \int \rho u_i, \int \rho\mathbf{u}\cdot\mathbf{u}, \int \rho \exp(\sum \lambda_i u_i), \lambda_i \in \mathbb{R}$
	Convectively filtered Burgers	
One dimensional	$u_t + \bar{u}u_x = 0$	$\int u, \int \bar{u}, TV(u), \|u\|_\infty$
Potential function	$\mathbf{u}_t + \bar{\mathbf{u}}\cdot\nabla\mathbf{u} = 0$, $\mathbf{u} = \nabla\phi$	$\int u_i, \int \bar{u}_i, \|\mathbf{u}\|_\infty$
Continuity equation	$\mathbf{u}_t + \bar{\mathbf{u}}\cdot\nabla\mathbf{u} = 0$, $\rho_t + \nabla(\rho\bar{\mathbf{u}}) = 0$	$\int \rho, \int \rho u_i, \int \rho\mathbf{u}\cdot\mathbf{u}, \|\mathbf{u}\|_\infty$

Using this and bounds (19) and (23), Young's inequality states

$$\left\| \frac{\partial}{\partial x_i} \bar{u}_j \right\|_{L^\infty} \leqslant \left\| \frac{\partial}{\partial x_i} g \right\|_{L^1} \|u_j\|_{L^\infty} \leqslant M \|u_{0_j}\|_{L^\infty},$$

which leads directly to the bound

$$\left\| \int_0^t \nabla \cdot \bar{\mathbf{u}}\, \mathrm{d}t \right\|_{L^\infty} \leqslant nM \max_j \|u_{0_j}\|_{L^\infty} t. \tag{24}$$

Thus for finite time, the Jacobian of ϕ remains uniquely invertible, with a continuously differentiable inverse and thus (20) is a unique $C^1(\mathbb{R}^n)$ solution to (16*a*)–(16*c*). □

Theorem 4.2. *Let* $g(\mathbf{x}) \in W^{1,1}(\mathbb{R}^n)$ *and* $\mathbf{u}_0(\mathbf{x}) \in L^\infty(\mathbb{R}^n)$*, then there exists a unique global solution* $\mathbf{u}(\mathbf{x}, t) \in L^\infty(\mathbb{R}^n, \mathbb{R})$ *to the initial-value problem (16a)–(16c).*

Proof. The proof is the same as for theorem 4.1. $\phi(\boldsymbol{\xi}, t)$ still has a unique continuously differentiable inverse, and the solution remains $\mathbf{u}(\mathbf{x}, t) = \mathbf{u}_0(\phi^{-1}(\mathbf{x}, t))$, but now lacks continuity due to the initial conditions. □

5. Invariants of motion

The inviscid and viscous Burgers equations have invariants of motion that are a result of their inherent geometric structure. Often these invariants of motion can only be realized with additional constraints which impart some physical meaning. These constraints are specifically: restriction to a single dimension, assuming the velocity is the gradient of a potential function, $\mathbf{u} = \nabla\phi$, and by the addition of a continuity equation. Both restricting to a single dimension and assuming a potential function establishes a curl free velocity. Introducing a continuity equation similar to that in the Euler equations introduces density. Table 2 shows the various invariants of motions for the equations under different constraints.

By restricting the inviscid Burgers equation to one dimension there are a countably infinite number of conserved quantities [47]. When the viscous Burgers equation is restricted to one

dimension, only the wave mass is conserved. Similarly, CFB conserves wave mass when restricted to one dimension [35]. This result is dependent upon the filter g being an even function, which was a criterion set down in section 3. In the special case of the Helmholtz filter, this quantity is also a Hamiltonian structure [35, 36].

One-dimensional CFB has an additional conserved quantity, total variation, that is not found in either the inviscid or the viscous Burgers equation. CFB can be considered a convection equation, with convective velocity $\bar{u}$. Since the solution is a remapping of the initial condition, the total variation remains constant over time. For continuous initial conditions and thus continuous solutions, this can be verified directly by noting that $T.V.(f) = \int |f_x| \, \mathrm{d}x$ for continuous functions. By taking the derivative of (7*a*) and integrating its absolute value, one obtains

$$\frac{\partial}{\partial t} \int |u_x| \, \mathrm{d}x + \int \mathrm{sgn}(u_x)(\bar{u}u_x)_x \, \mathrm{d}x = 0. \tag{25}$$

Break the second term into intervals where $\mathrm{sgn}(u_x)$ remains constant. u_x and $\bar{u}$ are continuous due to theorem 4.1, so where $\mathrm{sgn}(u_x)$ changes sign, $u_x = 0$. Thus the second term is zero and $\int |u_x| \, \mathrm{d}x$ remains constant over time. This was established by Bhat and Fetecau for the Helmholtz filters [36], but remains true for any filter satisfying theorem 4.1.

When assuming a potential function for the velocity, $\mathbf{u} = \nabla\phi$, in the inviscid and viscous Burgers equation wave mass is again conserved. Note that restriction to one dimension trivially implies a potential function for the velocity. Similarly, CFB conserves wave mass with the assumption of a potential function. The velocities $\mathbf{u}$ and $\bar{\mathbf{u}}$ have different potential functions related through the filter g. Again the conservation of wave mass is dependent on g being radially symmetric.

The addition of a continuity equation to the inviscid Burgers equation results in multiple invariants of motion [47]. It can be easily shown that this addition conserves mass, momentum and kinetic energy. An invariant of no known physical significance is additionally obtained and can be seen in table 2. CFB also conserves mass, momentum and kinetic energy when a continuity equation involving the filtered velocity is added.

CFB has another quantity that remains constant over time. As can be seen in the existence and uniqueness theorem in section 4, the infinity norm of the unfiltered velocity remains constant. Indeed both the maximum and minimum of the initial condition is preserved over time. This was shown for the one-dimensional case by Holm and Staley [35].

It should be noted that almost all of the invariants of motion are found using the unfiltered velocity. The filtered velocity, which is to be considered the physical quantity, has only wave mass preserved. In order for the filtered velocity to accurately model the macroscopic (low wave number) behavior, energy must be leaving the system in the high wave number spectrum. Indeed, numerical simulation in sections 9 and 10 shows that energy leaves the filtered velocity at the high wave numbers.

Besides wave mass, the filtered velocity does not appear in the invariants of motion. It was mentioned in the introduction that the filtered velocity is meant as the physically relevant quantity and is to capture the low wave number behavior. Thus it should not capture all of the energy behavior in the higher wave modes. The unfiltered velocity is intended to capture such behavior. Therefore the invariants of motion for the unfiltered velocity would be more properly compared to those of inviscid Burgers equations, just as the invariants of motion for the filtered velocity should be compared to those of the viscous Burgers equation. It should be noted that the inviscid Burgers equation can be thought of as a conservation law for the wave mass. Thus this invariant of motion is of primary importance and is noticeably preserved in viscous Burgers equations and in both velocities in the convectively filtered Burgers equation.

6. Traveling wave solutions

In this section, one-dimensional CFB, (7*a*) and (7*b*), is shown to have a traveling wave solution. For the Helmholtz filter, these have already been found by Bhat and Fetecau [36] and Holm and Staley [35]. This section generalizes the results to general filters. This traveling wave solution is a moving shock that handles an amplitude drop or increase. It satisfies the limiting boundary conditions

$$\lim_{x\to\infty} u(x,t) = u_r, \qquad \lim_{x\to-\infty} u(x,t) = u_l. \tag{26}$$

Inviscid Burgers is known to have weak solutions

$$u(x,t) = \begin{cases} u_l & x < ct \\ u_r & x \geqslant ct \end{cases} \tag{27}$$

with $c = \frac{1}{2}(u_r + u_l)$. The speed at which discontinuities travel is dictated by the Rankine–Hugoniot jump condition [15].

It is not difficult to show that (27) is a weak solution to one-dimensional CFB as well. With equation (27) as the unfiltered velocity solution, the filtered velocity is

$$\bar{u}(x,t) = (u_r - u_l)\int_{-\infty}^{x-ct} g^{\alpha}(s)\,\mathrm{d}s + u_l, \tag{28}$$

with g^{α} as the filter and $c = \frac{1}{2}(u_r + u_l)$. As filter g is an even function, the value of the filtered velocity in the middle of the shock is the speed of the shock, $\bar{u}(ct,t) = c$. This is crucial in verifying that (27) is a weak solution.

There are some notable properties of the traveling wave solution. It travels at the same speed as traveling wave solutions to inviscid Burgers. As it is desirable for CFB to capture wave speed accurately, this is promising. Additionally, as $\alpha \to 0$, the filter g approaches the Dirac delta function, thus (28) converges to (27), thus the traveling solutions to CFB converges to weak solutions of the inviscid Burgers equation.

It is also noted that when $u_l < u_r$ that the traveling wave solution will converge to a discontinuity, where $u(ct^-,t) < u(ct^+,t)$. The Lax entropy condition states that at points of discontinuity $u(x^-,t) > u(x^+,t)$. Thus the traveling wave solutions to CFB will converge to a weak solution of the inviscid Burgers equation which violates the entropy condition. This non-entropic behavior can be avoided by only allowing continuous initial conditions. This is shown in [48].

7. Numerics

For numerical simulations of equations (9*a*) and (9*b*) a pseudospectral method was utilized. Spatial derivatives and filtering were performed in the Fourier space. The equations were advanced in time using the optimal third-order TVD Runge–Kutta scheme presented by Gottlieb and Shu [49]. We have also conducted runs with the classic Runge–Kutta 4 and the Runge–Kutta–Fehlberg method with virtually identical results for the initial conditions and time lengths examined here. The CFL coefficient was chosen at $c = 0.3$, with runs typically conducted at resolutions of $2^{12} = 4096$ for one dimension and 256×256 for two dimensions. Aliasing errors were handled using the same technique as in Holm and Staley [35].

It should be noted that this numerical method captures the large scale behavior in both the unfiltered and filtered velocity for an initial period. The filtered velocity is considered the physically relevant quantity and requires less resolution to capture. Because it should require less resolution, a numerical method that would resolve only the filtered velocity using

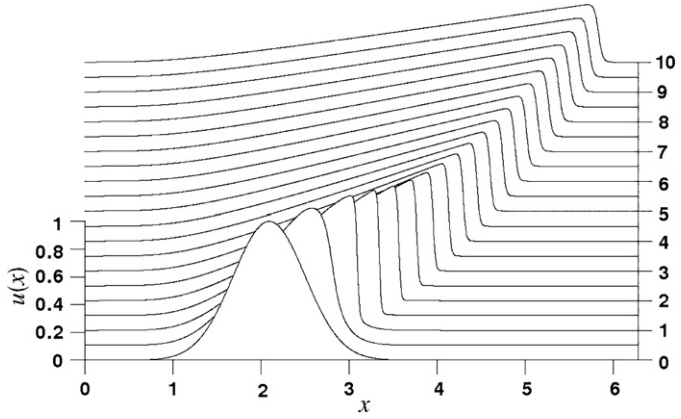

Figure 2. Evolution of a Gaussian distribution under the viscous Burgers equation for $t = 0, \ldots, 10$. The viscosity is $\nu = 0.005$.

equation (8) would probably be more efficient. However, since our initial priority in this effort lies in exploring the properties of CFB rather than in making efficient simulations, the scheme was designed to capture both velocities.

Our groups have extensive experience in using such techniques with the LAE-α and LANS-α simulations where the accuracy and stability of the approach have been established [5]. Of particular interest, we have shown that the H^1 norm of the energy in LAE-α computations are numerically conserved in longtime calculation [5].

8. Shock behavior

8.1. Unfiltered velocity

In section 4, it was proven that the unfiltered velocity has a continuous derivative for all time. This was shown by proving that the Jacobian of the material map remains nonzero. In equation (22) the Jacobian is shown to have an exponential structure. As it happens the Jacobian remains nonzero, but approaches zero rapidly. From a method of characteristics point of view, the characteristics are growing continuously closer, but never intersect. Thus the unfiltered velocity will form shocks of continually smaller thickness. In numerical simulations, this process will inevitably drop below the finite resolution, thus from a numerical perspective, the unfiltered velocity becomes discontinuous. The filtered velocity, however, appears continuous in the numerical simulations. The shocks in the filtered velocity will not drop below the resolution of the numerical run provided a large enough α has been chosen. For the average run, α is chosen to be at least a magnitude greater than Δx. This puts approximately 15 points across the width of the shock, which seems a reasonable number to resolve its features.

8.2. Shock profile

In the 1D viscous Burgers equation, a wave will propagate to the right, with the higher velocities overcoming the lower velocities, creating steep gradients. This steepening continues until a balance with dissipation is reached. Figure 2 shows the evolution of the viscous Burgers equation with a Gaussian distribution as an initial condition.

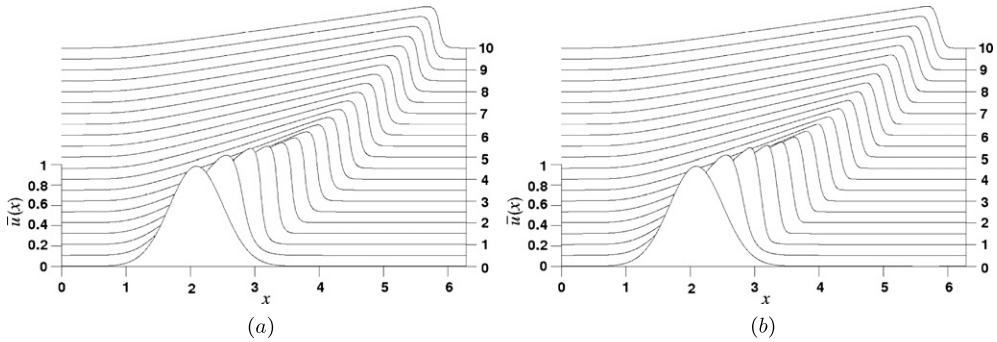

Figure 3. Evolution of CFB using different filters from $t = 0, \ldots, 10$. Only the filtered velocity is shown. For all filters $\alpha = 0.05$. (*a*) Helmholtz filter $g(x) = \frac{1}{2}\exp(-|x|)$. (*b*) Gaussian filter $g(x) = \pi^{-1/2}\exp(-x^2)$.

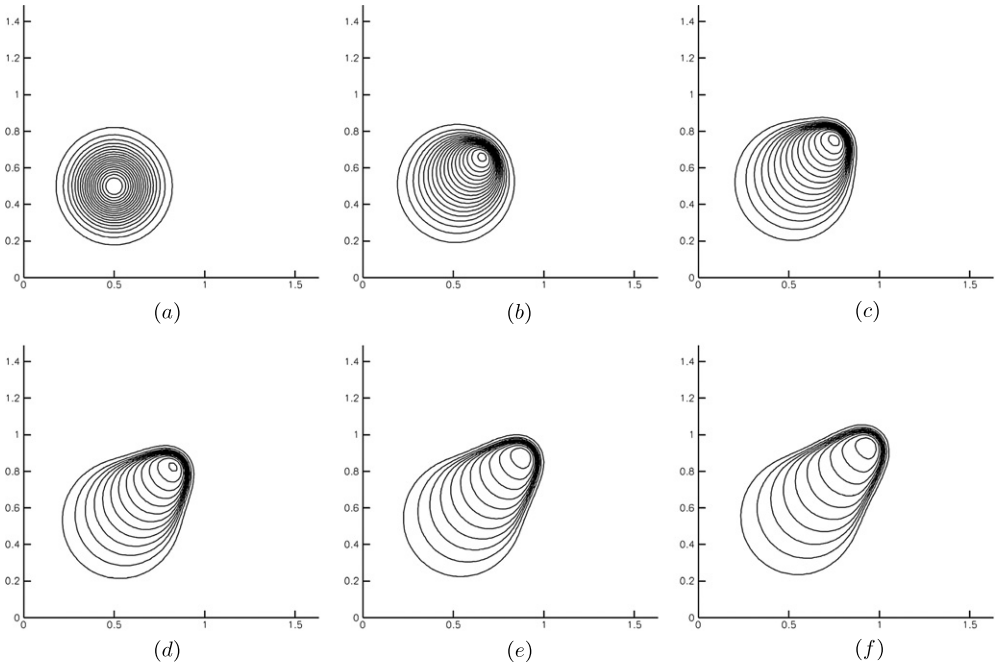

Figure 4. Contour plots showing the evolution of 2D CFB using a Helmholtz filter with a Gaussian pulse as the initial condition. $\alpha = 0.08$ with 128×128 gridpoints.

In figure 3, the evolution of CFB can be seen for two filters. The behavior is qualitatively the same as the viscous Burgers equation in reference to wave propagation and shock formation. Every filter that has been numerically simulated has shown similar behavior.

Numerical simulations were also conducted in two dimensions. It is more difficult to show shock formation in 2D, but figures 4 and 5 show the evolution of a pulse under the Helmholtz and Gaussian filter. In both runs, the pulse moves up and to the right, becoming steeper, but never forming a discontinuity. Once the shock has formed, the pulse begins to decrease in amplitude.

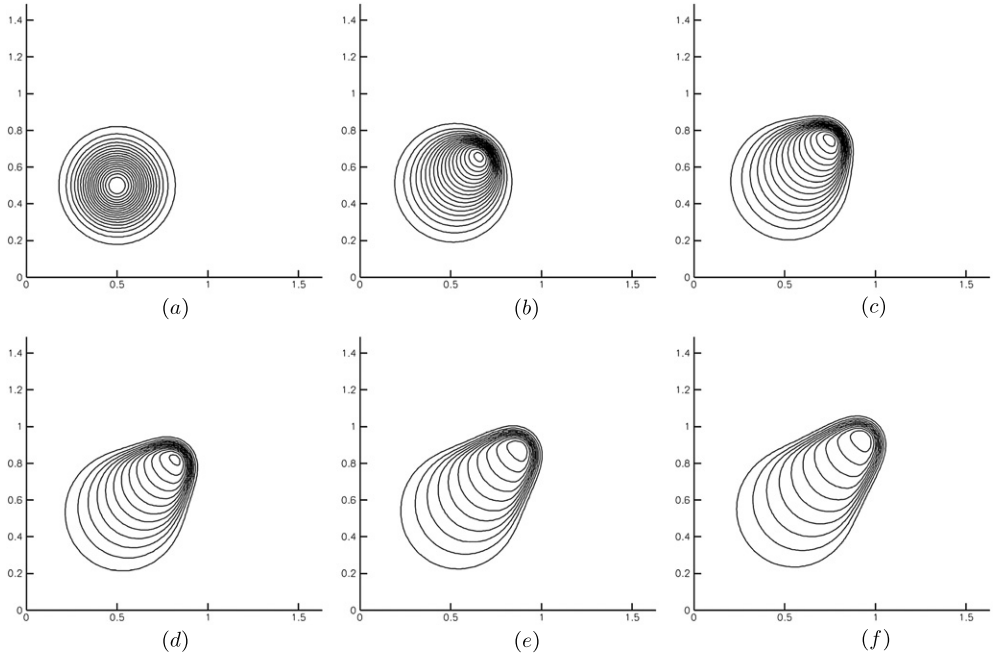

Figure 5. Contour plots showing the evolution of 2D CFB using a Gaussian filter with a Gaussian pulse as the initial condition. $\alpha = 0.08$ with 128×128 gridpoints.

8.3. Shock thickness

One of the characteristics of the viscous Burgers equation is that as ν becomes smaller, the shocks formed by the solution become thinner and steeper. Heuristically, smaller ν's allow more energy into higher wavemodes, which causes a steeper gradient.

Numerical simulations were run for various values of α and various filters in equations (9*a*) and (9*b*), to examine the effects upon shock thickness. Smaller α correlates with less dampening in the high wavemodes, thus allowing steeper shocks much like the effect of the viscous term. Figure 6(*a*) shows shocks for the Helmholtz filter for different values of α. As α decreases the shocks get thinner. Similar results hold true for all filters and simulations made in two dimensions.

Shock thickness can be examined analytically by looking at the traveling wave solution. Here the thickness of the shock is defined to be the length over which 90% of the amplitude change takes place, centered at the center. From section 6, the traveling wave solution is

$$\bar{u}(x,t) = (u_r - u_l) \int_{-\infty}^{x-ct} g^{\alpha}(s)\,\mathrm{d}s + u_l.$$

The thickness of the shock will then be $2\alpha b$, where b is the value where

$$\int_{-b}^{b} g(x)\,\mathrm{d}x = \int_{-\alpha b}^{\alpha b} \frac{1}{\alpha} g\left(\frac{x}{\alpha}\right)\,\mathrm{d}x = 0.9. \tag{29}$$

This length is independent of u_r and u_l. As such, the thickness of the shock varies linearly on the parameter α. Figure 6(*b*) shows shock thickness versus α for different filters.

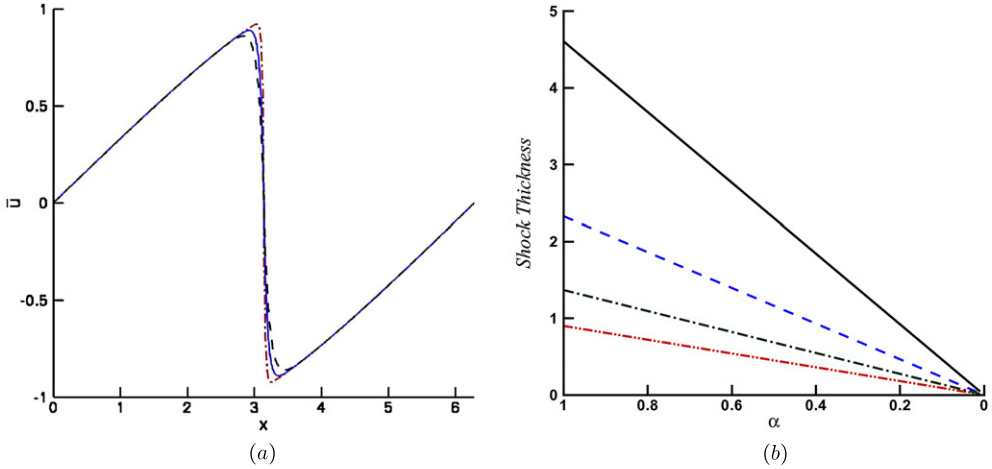

(*a*) (*b*)

Figure 6. The thickness of the shocks formed in CFB vary depending upon the value of α. (*a*) As α decreases the thickness of the shock decreases. $\alpha = 0.08 =$ - - - -, $\alpha = 0.05 =$ ——, $\alpha = 0.02 = - \cdot - \cdot -$. (*b*) The thickness of the traveling shock decreases linearly with α. Helmholtz filter, $g(x) = \frac{1}{2}\exp(-|x|) =$ ——, Gaussian filter, $g(x) = \pi^{-1/2}\exp(-x^2) =$ - - - -, Hat filter, $g(x) = \{x - 1 \text{ for } x \in (-1, 0), 1 - x \text{ for } x \in (0, 1), 0 \text{ otherwise}\} =$ — · —, Tophat filter, $g(x) = \{1 \text{ for } x \in [-\frac{1}{2}, \frac{1}{2}], 0 \text{ otherwise}\} =$ — · · —.

9. Spectral energy

Analytically CFB has been examined on an infinite domain. This is of course impossible numerically, so in numerical experiments, simulations were performed on the domains $[0, 2\pi]$ and $[0, 2\pi] \times [0, 2\pi]$ for one and two dimensions, with periodic boundary conditions. Since simulations were performed with a pseudospectral method, the spectral energy decompositions were easily obtained.

The examination of the spectral energy decompositions begins by stating a special case of Sobelev embedding theorem that is found in Hunter and Nachtegaele [50]. There it is stated that for a function $f : \mathbb{T}^n \to \mathbb{C}$ defined by

$$f(\mathbf{x}) = \sum_{\mathbf{m}\in\mathbb{Z}^n} a_{\mathbf{m}}\, \mathrm{e}^{\mathrm{i}\mathbf{m}\cdot\mathbf{x}}$$

that if

$$\sum_{\mathbf{m}\in\mathbb{Z}^n} |\mathbf{m}|^{2p}|a_{\mathbf{m}}|^2 < \infty \tag{30}$$

for some $p > \frac{n}{2}$ then f is continuous. Furthermore if condition (30) holds true for $p > j + \frac{n}{2}$ then f has j continuous derivatives.

If spectral energy $E(k)$ is defined as

$$E(k) = \sum_{|\mathbf{m}|=k} |a_{\mathbf{m}}|^2, \tag{31}$$

then (30) can then be rewritten as

$$\sum_{k=0}^{\infty} k^{2p} E(k) < \infty. \tag{32}$$

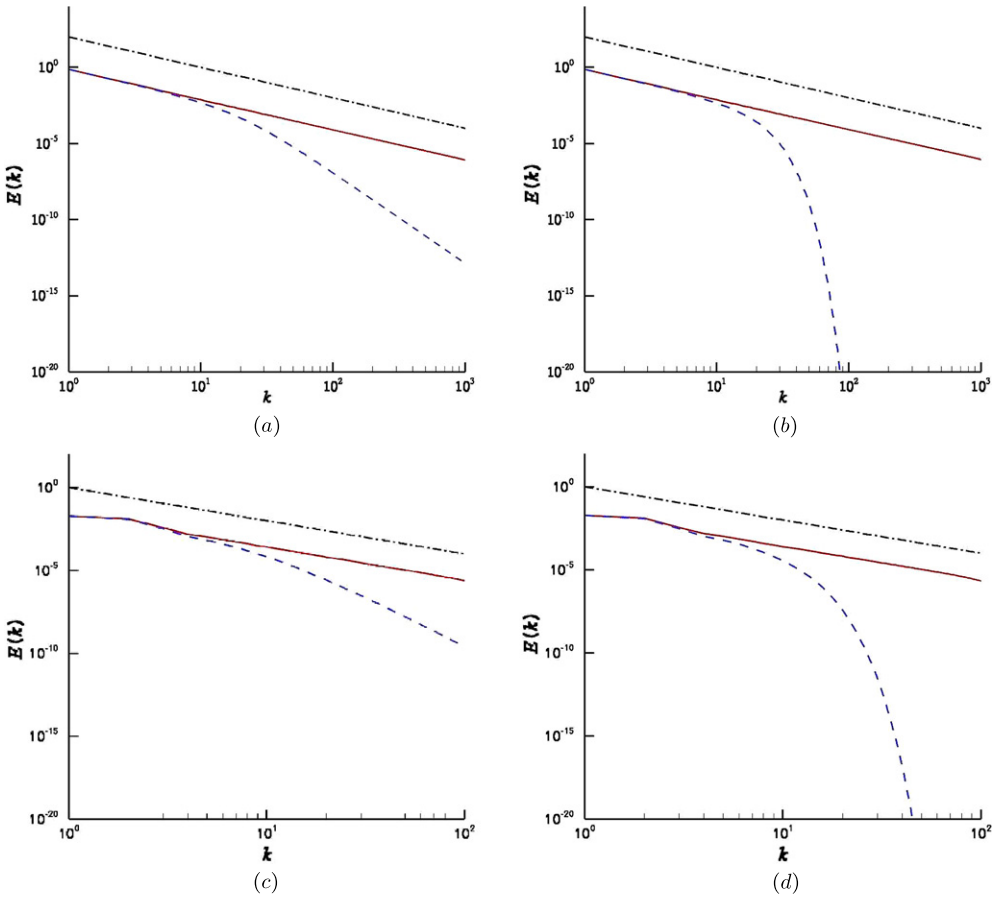

Figure 7. Spectral energy decompositions for 1D and 2D CFB using Helmholtz and Gaussian filters. All simulations were performed with $\alpha = 0.08$. (*a*) and (*b*) are one-dimensional simulations at $t = 3$ with initial conditions $u(x) = \sin(x)$ for Helmholtz and Gaussian filters respectively. In figure (*a*) one can see that the energy cascade slope drops dramatically after wavelength $\frac{1}{\alpha}$. This occurs similarly in figure (*b*), with the exception that the spectral energy decreases exponentially due to the Gaussian filter. (*c*) and (*d*) are two-dimensional simulations at $t = 1$ with Gaussian pulses as the initial conditions, again with Helmholtz and Gaussian filters respectively. The spectral energy decompositions show similar characteristics as the one-dimensional simulations. The spectral energy of $\mathbf{u}$ ——, $\bar{\mathbf{u}}$ - - - - and a reference slope of -2 — · — are shown.

Thus it can be seen that the rate at which $E(k)$ decays as $k \to \infty$, can determine the smoothness of the equation. In one dimension, if $E(k)$ decays faster than $\frac{1}{k^2}$, continuity is guaranteed. In a logarithmic plot, this correlates with an energy cascade slope of less than -2. In n dimensions, if $E(k)$ decays faster than $\frac{1}{k^{n+1}}$ (energy cascade slope less than $-(n+1)$) continuity is guaranteed. Existence of continuous derivatives can be guaranteed in a similar fashion.

Inviscid Burgers and viscous Burgers (in its inertial frame) have been shown to have an energy cascade slope of -2 during shock formation [44, 45]. Numerical simulations suggest that CFB also has an energy cascade slope of -2 for the unfiltered velocity, independent of filter and dimension. The filtered velocity's energy cascade slope is then highly dependent upon the filter employed. In figure 7, the spectral energy decompositions for simulations with

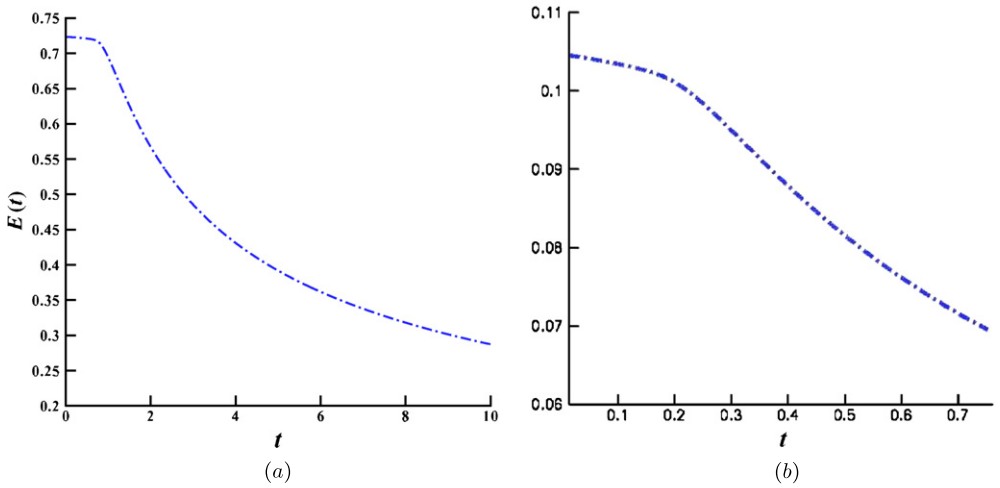

Figure 8. Energy decay for the 1D and 2D viscous Burgers equations. (*a*) The energy decay for the 1D viscous Burgers equation. Initial conditions $u(x, 0) = \exp(-3x^2)$, with $\nu = 0.001$ and 1024 gridpoints. (*b*) The energy decay for the 2D viscous Burgers equation. Initial conditions $u_1(x, y, 0) = \exp(-30x^2 - 30y^2)$ and $u_2(x, y, 0) = \exp(-30x^2 - 30y^2)$, with $\nu = 0.001$ and 128×128 gridpoints; $\int \mathbf{u} \cdot \mathbf{u}$ — · —.

the Helmholtz and Gaussian filter in one and two dimensions are shown. The spectral energy decompositions are shown for a time well after the shocks are fully developed. The -2 energy cascade slope is clearly seen, as well as the effect of the filters on the filtered velocity's energy cascade slope. The Helmholtz filtered velocity displays a -6 energy cascade slope for high wave numbers, guaranteeing a continuous derivative in one and two dimensions. The Gaussian filtered velocity decays faster than any polynomial for high wave numbers, thus guaranteeing infinite continuous derivatives. This is similar to the solutions of the viscous Burgers equation. The viscosity term causes an exponential drop in the energy spectrum at high wave numbers, also guaranteeing infinite continuous derivatives.

In section 4, the unfiltered velocity and thus the filtered velocity were proven to have a continuous derivative for continuously differentiable initial conditions. In section 8.1, it was suggested that despite this, the unfiltered velocity can form shocks that will grow narrower than any finite resolution. Thus for numerical purposes the unfiltered velocity can be considered discontinuous. The filtered velocity will appear continuous to numerical simulations if the energy cascade slope satisfies conditions dictated by the special case of the Sobolev embedding theorem mentioned.

10. Energy norms

The kinetic energy for the Burgers equation can be defined as $\int \frac{1}{2}\mathbf{u} \cdot \mathbf{u}$. In CFB, there are two different velocities presenting three different kinetic energies: $\int \frac{1}{2}\mathbf{u} \cdot \mathbf{u}$, $\int \frac{1}{2}\mathbf{u} \cdot \bar{\mathbf{u}}$ and $\int \frac{1}{2}\bar{\mathbf{u}} \cdot \bar{\mathbf{u}}$. Analytical comparisons between the energy decay rates of the viscous Burgers equation and CFB have proven fruitless with the exception of the one-dimensional case using the Helmholtz filter. In one dimension, the nonlinear term is more easily handled, and the Helmholtz filter (10*b*) provides a convenient inverse, allowing greater manipulation capabilities.

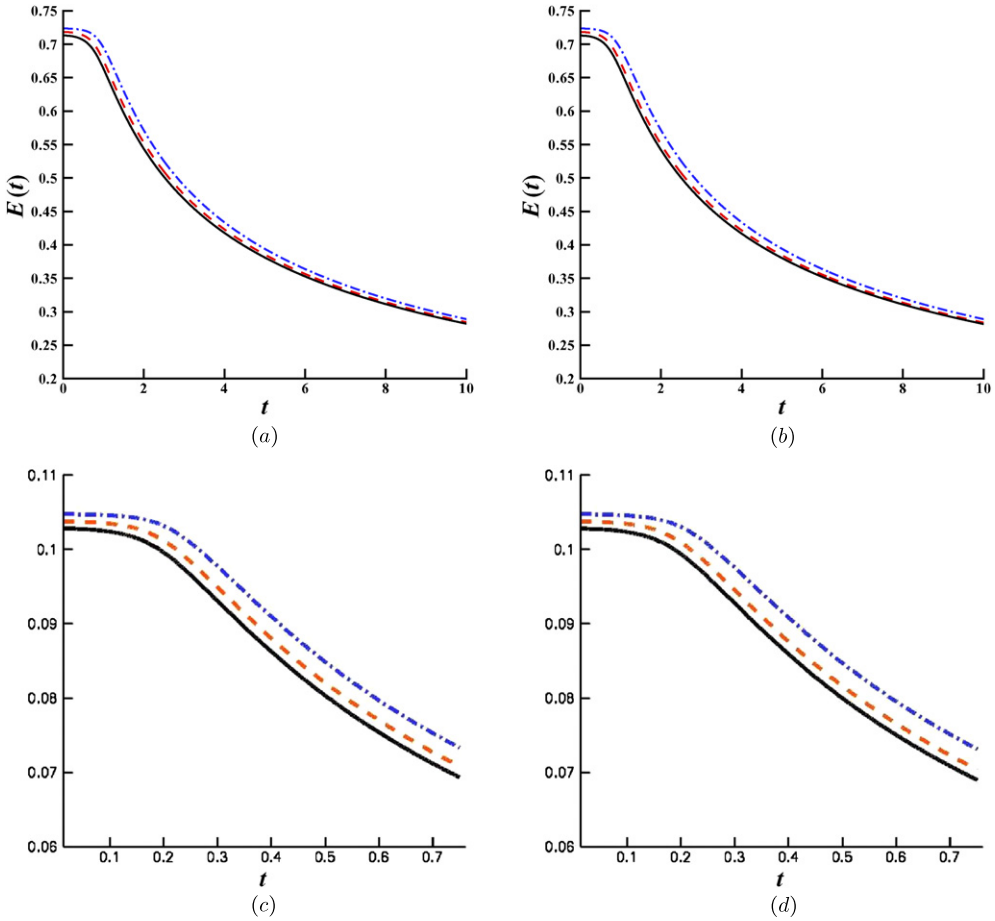

Figure 9. Energy decay for 1D and 2D CFB. $\int \mathbf{u}\cdot\mathbf{u}$ — · —, $\int \mathbf{u}\cdot\bar{\mathbf{u}}$ - - - -, $\int \bar{\mathbf{u}}\cdot\bar{\mathbf{u}}$——. Figures (*a*) and (*b*) show the energy decay for 1D CFB with the Helmholtz and Gaussian filter respectively. Initial conditions $u(x,0) = \exp(-3x^2)$, with $\alpha = 0.05$ and 1024 gridpoints. Figures (*c*) and (*d*) show the energy decay for 2D CFB with the Helmholtz and Gaussian filter. Initial conditions $u_1(x,y,0) = \exp(-30x^2 - 30y^2)$ and $u_2(x,y,0) = \exp(-30x^2 - 30y^2)$, with $\alpha = 0.05$ and 128×128 gridpoints. Decay rates are similar to those seen in figure 8.

For the one-dimensional viscous Burgers equation, kinetic energy can be defined as

$$E(t) = \int \frac{u(x,t)^2}{2}\,\mathrm{d}x. \tag{33}$$

The decay rate of the energy is easily calculated to be

$$\frac{\mathrm{d}}{\mathrm{d}t}\int \frac{u^2}{2}\,\mathrm{d}x = -\nu\int u_x^2\,\mathrm{d}x. \tag{34}$$

For one-dimensional CFB using the Helmholtz filter, the energy decay rates are

$$\frac{\mathrm{d}}{\mathrm{d}t}\int \frac{u^2}{2}\,\mathrm{d}x = \alpha^2\int \frac{(\bar{u}_x)^2}{4}(\bar{u}_x + u_x)\,\mathrm{d}x \tag{35a}$$

$$\frac{\mathrm{d}}{\mathrm{d}t}\int \frac{\bar{u}u}{2}\,\mathrm{d}x = \alpha^2\int (\bar{u}_x)^3\,\mathrm{d}x \tag{35b}$$

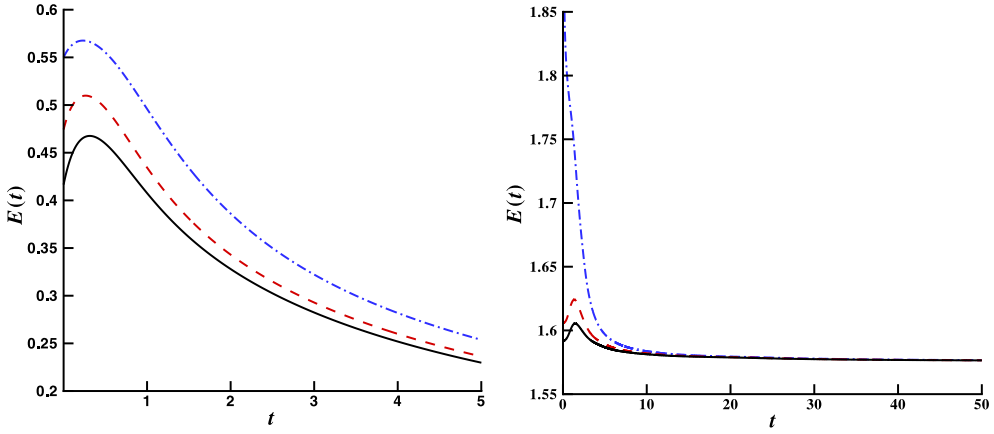

Figure 10. Here the energies for CFB are shown. $\int \mathbf{u}\cdot\mathbf{u}$ — · —, $\int \mathbf{u}\cdot\bar{\mathbf{u}}$ - - - -, $\int \bar{\mathbf{u}}\cdot\bar{\mathbf{u}}$ ——. In (a) the initial conditions are $u_0 = C(x-\pi)/(1+100(x-\pi)^4)$, with C chosen such that $\max(u_0) = 1$, and (b) with a random initial condition. In both cases the energies increase initially, but then behave with normal energy decaying behavior.

$$\frac{\mathrm{d}}{\mathrm{d}t}\int \frac{\bar{u}^2}{2}\,\mathrm{d}x = -3\alpha^2 \int \bar{u}_x \bar{u}_{xx}\left(I-\alpha^2\partial_x^2\right)^{-1}(\bar{u})\,\mathrm{d}x. \tag{35c}$$

Here a similarity in structure can be seen, especially when comparing (34) with (35*b*). The integrands of both are the first derivatives of velocities, implying that the majority of the energy is lost through steep gradients, a common concept. The similarity is interesting considering that in the one-dimensional viscous Burgers equation, the energy is lost through the viscous term, while the energy is lost in the nonlinear term for one-dimensional CFB.

Numerical simulations were conducted for both viscous Burgers equation and CFB in one and two dimensions. Figure 8 shows the energy decay rates for the viscous Burgers equation. Figure 9 shows the energy decay rates for CFB using the Helmholtz and Gaussian filters. In figure 9, it can be seen that the different kinetic energies tend toward each other with primary difference occurring in amplitude. Comparing figures 8 and 9, it is seen that the energy decay rates behave quantitatively similar between the CFB and viscous Burgers equations. Energy decay is minimal until the formation of a shock and then the energy decreases rapidly upon formation of the shock.

10.1. Energy can increase

It is also important to note that equations (35*a*)–(35*c*) are not sign definite as is equation (34). This shows while the energy for the viscous Burgers equation must always decrease, CFB can experience an increase in energy. Specifically, it can be seen in equation (35*b*), that for steep decreasing gradients energy will be lost, but for steep increasing gradients energy will be gained. However, due to the nature of the equation increasing gradients will decrease in steepness, while decreasing gradients will increase or remain steep. This can be seen in the evolution of a Gaussian pulse, as in figure 3. Thus any increase in energy should be brief.

One would also suspect that as $\alpha \to 0$ that the brief energy increase would disappear. If solutions to CFB are, in fact, limiting to solutions of the inviscid Burgers equation, then it follows that the energy rates would approach those of the inviscid Burgers equation, as well.

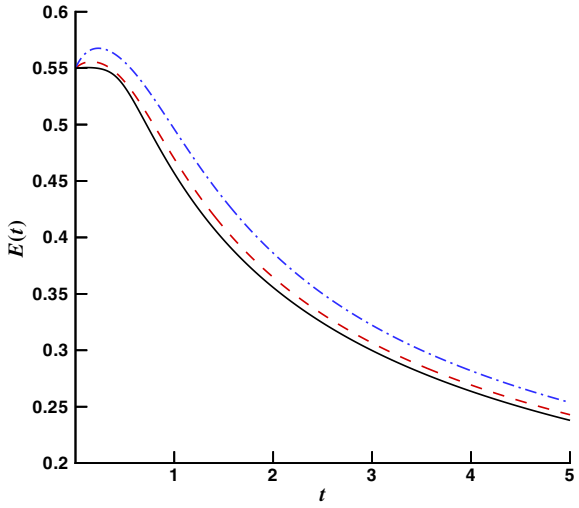

Figure 11. The energy $\int \mathbf{u} \cdot \mathbf{u}$ is compared for three different values of α. $\alpha = 0.08$ — · —, $\alpha = 0.05$ - - - and $\alpha = 0.02$ ——. The initial conditions are $u_0 = C(x-\pi)/(1+100(x-\pi)^4)$, with C chosen such that $\max(u_0) = 1$. For all three values of α there is a brief increase of energy, but as α becomes smaller, this increase in energy becomes less substantial.

Figure 10 shows two numerical simulations where the initial conditions were chosen to generate an increase in energy. In both cases the energy will briefly rise before beginning to decay as expected. Figure 11 shows three simulations with decreasing α. As was expected, the brief increase in energy becomes less dramatic as α decreases.

11. Conclusion

By passing the convective velocity through a low-pass filter, the cascade of energy into higher wave modes of the inviscid Burgers equation has been slowed down after the preselected length scale. It has been proven that for a general class of filters, solutions to equations (9*a*) and (9*b*) exist and are unique. Furthermore, for continuous initial conditions the solution remains continuous for all time. Much of the geometric structure of the inviscid Burgers equation seen in invariants of motion is preserved in the averaging process. We have found traveling wave solutions that propagate at the correct wave speed, and converge to weak solutions of the inviscid Burgers equation.

Through numerical simulations, much of the behavior of CFB has been examined. For smooth initial conditions, such as Gaussian pulses and sine waves, the wave profile behavior of the CFB and that of the viscous Burgers equation are qualitatively similar. This similarity is believed to come about because the CFB and viscous Burgers equations both converge to the entropy solution of the inviscid Burgers equation for such initial conditions. The convergence of CFB to the entropy solution is under investigation and will be shown in [48].

The thickness of shocks formed under the CFB equations has been shown to be regulated by the parameter α, which is the characteristic width of the filter. Spectral energy decompositions have given insight into how the high wavemodes are handled and what filters are needed to guarantee the smoothness of the solution.

Energy norms behave similarly to those in the viscous Burgers equation, in that the energy is shown to be lost upon shock formation and lost through steep gradients. A significant difference is found between the two in that CFB can have a brief increase in energy for certain initial conditions. This increase is brief and appears to disappear in the limit as $\alpha \to 0$.

All together, filtering the convective velocity appears to be a valid technique for high wavemode regularization. More work is still needed in several areas. Convergence to the entropy solution is being established and is under investigation. Further numerical experiments are needed, specifically in long-time simulations and more complex flows in 1D and in multiple dimensions. Hopefully these questions will be addressed and this regularization can be extended into more general fluid dynamics equations.

Acknowledgments

The research in this paper was partially supported by the AFOSR contract FA9550-05-1-0334.

References

[1] Cheskidov A, Holm D D, Olson E and Titi E S 2004 On a Leray-α model of turbulence *Proc. R. Soc. Lond. Ser. A: Math. Phys. Eng. Sci.* **461** 629–49
[2] Foias C, Holm D D and Titi E S 2001 The Navier–Stokes-α model of fluid turbulence *Phys. D.* **152–3** 505–19
[3] Foias C, Holm D D and Titi E S 2002 The three dimensional viscous Camassa–Holm equations, and their relation to the Navier–Stokes equations and turbulence theory *J. Dyn. Diff. Eqns* **14** 1–35
[4] Marsden J E and Shkoller S 2001 Global well-posedness of the LANS-α equations *Proc. R. Soc. Lond.* **359** 1449–68
[5] Mohseni K, Kosović B, Shkoller S and Marsden J E 2003 Numerical simulations of the Lagrangian averaged Navier–Stokes (LANS-α) equations for homogeneous isotropic turbulence *Phys. Fluids* **15** 524–44
[6] Zhao H and Mohseni K 2005 A dynamic model for the Lagrangian averaged Navier–Stokes-α equations *Phys. Fluids* **17** 075106
[7] Mohseni K, Zhao H and Marsden J Shock regularization for the Burgers equation *AIAA Paper 2006-1516, 44th AIAA Aerospace Sciences Meeting and Exhibit (Reno, Nevada, Jan. 9–12 2006)*
[8] Bhat H S, Fetecau R C, Marsden J E, Mohseni K and West M 2005 Lagrangian averaging for compressible fluids *SIAM J. Multiscale Model. Simul.* **3** 818–37
[9] Holm D D, Marsden J E and Ratiu T S 1998 Euler–Poincaré models of ideal fluids with nonlinear dispersion *Phys. Rev. Lett.* **349** 4173–7
[10] Chen S Y, Holm D D, Margoin L G and Zhang R 1999 Direct numerical simulations of the Navier–Stokes-α model *Physica* D **133** 66–83
[11] Burgers J M 1948 A mathematical model illustrating the theory of turbulence *Adv. Appl. Mech.* **1** 171–99
[12] Lighthill M J 1956 Viscosity effects in sound waves of finite amplitude *Surv. Mech.* 250–351
[13] Cole J D 1951 On a linear quasilinear parabolic equation in aerodynamics *Q. Appl. Math.* **9** 225–36
[14] Whitham G B 1974 *Linear and Nonlinear Waves* (New York: Wiley)
[15] Lax P D 1973 *Hyperbolic Systems of Conservation Laws and the Mathematical Theory of Shock Waves* (Philadelphia, PA: SIAM)
[16] Gotoh T and Kraichnan R H 1993 Statistics of decaying Burgers turbulence *Phy. Fluids* A **5** 445–57
[17] Holm D D and Geurts B J 2006 Alpha-modeling strategy for LES of turbulent mixing **39** 2213–29
[18] Tadmor E 2004 Burgers equation with vanishing hyper-viscosity *Commun. Math. Sci.* **2** 317–24
[19] Oberai A A and Wanderer J 2006 A dynamic multiscale viscosity method for the spectral approximation of conservation laws *Comp. Methods Appl. Mech. Eng.* **195** 1778–92
[20] Oleinik O A 1957 Discontinuous solutions and non-linear differential equations *Am. Math. Soc. Transl.* **26** 95–172
[21] Kruzkov S N 1970 First order quasilinear equations in several independent variables *Math. USSR Sbornik* **10** 217–43
[22] De Lellis C 2004 Minimal entropy conditions for Burgers equation *Q. Appl. Math.* **64** 687–700
[23] Hopf E 1950 The partial differential equation $u_t + uu_x = \mu u_{xx}$ *Commun. Pure Appl. Math.* **3** 201–30

[24] Lattanzio C and Marcati 2003 Global well-posedness and relaxation limits of a model for radiating gas *J. Diff. Eqns* **190** 439–65
[25] Liu H and Tadmor E 2001 Critical thresholds in a convolution model for nonlinear conservation laws *SIAM J. Math. Anal.* **33** 930–45
[26] Schochet S and Tadmor E 1992 The regularized Chapman–Enskog expansion for scalar conservation laws *Arch. Ration. Mech. Anal.* **119** 95–107
[27] Kondo C I and Lefloch P G 2002 Zero diffusion–dispersion limits for scalar conservation laws *SIAM J. Math Anal.* **33** 1302–29
[28] Lax P D and Levermore C D 1983 The small dispersion limit of the KdV equations: III *Commun. Pure Appl. Math.* **XXXVI** 809–30
[29] Kakutani T and Kawahara T 1970 Weak ion-acoustic shock waves *J. Phys. Soc. Japan* **29** 1068–73
[30] Gurevich A V and Pitaevskii L P 1974 Nonstationary structure of a collisionless shock wave *Sov Phys—JETP* **38** 291–7
[31] Germano M, Piomelli U, Moin P and Cabot W H 1991 A dynamic subgrid scale eddy viscosity model *Phys. Fluids* A **3** 1760–5
[32] Lesieur M and Metais O 1996 New trends in large-eddy simulations of turbulence *Annu. Rev. Fluid Mech.* **28** 45–82
[33] Hughes T J R, Mazzei L and Oberai A A 2001 Large eddy simulation of turbulent channel flows by the variational multiscale method *Phys. Fluids* **13** 1784–99
[34] Zhao H, Mohseni K and Marsden J 2004 Isotropic Lagrangian averaged Navier–Stokes-α equations with a dynamically calculated α *IMECE 2004-61591, 2004 ASME International Mechanical Engineering Congress and RD&D Expo (Anaheim, CA, Nov. 15–21 2004)*
[35] Holm D D and Staley M F 2003 Wave structures and nonlinear balances in a family of evolutionary PDEs *SIAM J. Appl. Dyn. Syst.* **2** 323–80
[36] Bhat H S and Fetecau R C 2006 A Hamiltonian regularization of the Burgers equation *J. Nonlinear Sci.* **16** 615–38
[37] Leray J 1934 Sur le mouvement d'un liquide visqueux emplissant l'espace *Acta Math.* **63** 193–248
[38] Ilyin A A, Lunasin E M and Titi E S 2006 A modified Leray-α subgrid scale model of turbulence *Nonlinearity* **19** 879–97
[39] van Reeuwijk M, Jonker H J J and Hanjali K 2006 Incompressibility of the Leray-α model for wall-bounded flows *Phys. Fluids* **18** 1–4
[40] Degasperis A, Holm D D and Hone A N W 2003 Integrable and non-integrable equations with peakons *Nonlinear Physics: Theory and Experiment II (Gallipoli, 2002)* (River Edge, NJ: World Scientific) pp 37–43
[41] Norgard G and Mohseni K 2007 A regularization of Burgers equation using a filtered convective velocity *AIAA paper 2007-0714, 45th AIAA Aerospace Sciences Meeting and Exhibit (Reno, Nevada, Jan. 8–11 2007)*
[42] Norgard G and Mohseni K 2007 Convectively filtered Burgers in one and multiple dimensions *AIAA paper 2007-4221, 37th AIAA Fluid Dynamics Conference and Exhibit (Miami, FL, Jun. 25–28 2007)*
[43] Bradshaw P 1976 *Turbulence* (Berlin: Springer)
[44] Kraichnan R H 1968 Lagrangian-history statistical theory for Burgers' equation *Phys. Fluids* **11** 265–77
[45] Gurbatov S N, Simdyankin S I, Aurell E, Frisch U and Toth G 1997 On the decay of Burgers turbulence *J. Fluid Mech.* **344** 339–74
[46] Aris R 1962 *Vectors, Tensors, and the Basic Equations of Fluid Mechanics* (Englewood Cliffs, NJ: Prentice-Hall)
[47] Davoudi J, Masoudi A A, Reza Rahimi Tabar M, Reza Rastegar A and Shahbazi F 2001 Three-dimensional forced Burgers turbulence supplemented with a continuity equation *Phys. Rev.* E **63** 056308
[48] Norgard G and Mohseni K 2008 Convergence of convectively filtered Burgers equation to the entropy solution of inviscid Burgers equation (unpublished). Online at http://arxiv.org/abs/0805.2176
[49] Gottlieb S and Shu C 1998 Total variation diminishing Runge–Kutta schemes *Math. Comput.* **67** 73–85
[50] Hunter J K and Nachtergaele B 2001 *Applied Analysis* (Singapore: World Scientific)